Space-time approach to microstructure selection in solid-solid transitions

Surajit Sengupta[1,2], Jayee Bhattacharya[2],Madan Rao[3,4]
[1] *Centre for Advanced Materials, Indian Association for the Cultivation of Science, Jadavpur, Kolkata 700032, India*
[2] *Advanced Materials Research Unit, S. N. Bose National Centre for Basic Sciences, Salt Lake, Kolkata 700091, India*
[3] *Raman Research Institute, C.V. Raman Avenue, Bangalore 560080, India*
[4] *National Centre for Biological Sciences (TIFR), Bellary Road, Bangalore 560065, India*

Nucleation of a solid in solid is initiated by the appearance of distinct dynamical heterogeneities, consisting of 'active' particles whose trajectories show an abrupt transition from ballistic to diffusive, coincident with the discontinuous transition in microstructure from a *twinned martensite* to *ferrite*. The active particles exhibit intermittent jamming and flow. The nature of active particle trajectories decides the fate of the transforming solid – on suppressing single particle diffusion, the transformation proceeds via rare string-like correlated excitations, giving rise to twinned martensitic nuclei. We characterize this transition using a thermodynamics in the space of trajectories in terms of a dynamical action for the active particles confined by the inactive particles.

PACS numbers: 64.70.K-,81.30.-t,83.60.-a,64.70.P-

A quench across a solid-solid transformation generally results in a product solid with specific microstructure – a long-lived, mesoscale ordering of atoms [1, 2] driven far from equilibrium. Crystallographic mismatch, usually present at the growing product-parent interface needs to accommodated dynamically to preserve continuity. This may happen in a variety of ways, giving rise to myriads of possible microstructures depending on the quench protocol (history). Commonly characterized microstructures like *ferrite* and *twinned martensite* [1–3] differ greatly. While ferrite is associated with a disorderly (or "civilian") movement of atoms, martensite is characterized by a coordinated (or "military") motion[1, 2], often resulting in alternating variants of the product sharing a common crystallographic mirror plane (twins) [3]. Relating multiscale physics, from atomic trajectories to mesoscale ordering, makes the study of microstructure selection particularly challenging. Here, we show that accommodation of interfacial mismatch occurs by the appearance of dynamical heterogeneities in the transforming solid. A thermodynamics of space-time trajectories of active particles[4, 5], represented by a dynamical action[6, 7] is used to describe a sharp transition in microstructure resembling ferrite to martensite as single particle diffusion is suppressed. The distribution of a space-time order parameter characterizing the nature of trajectories of active particles shows an abrupt change coinciding with this microstructural transition. Active particles exhibit intermittent jamming and flow showing that the underlying physics shares common features with the physics of plasticity[8, 9], glass[4, 10] and granular systems[11–13].

Our model two dimensional (2d) solid[14], analyzed using a molecular dynamics (MD) simulation[19], consists of particles confined within a box and interacting via an effective potential which is a sum of an anisotropic 2-body and 3- body potentials[15], constructed so as to produce a $P4m \to P2$ (square→rhombus) transition as the temperature or strength of the potential is varied at fixed density, Fig. 1 a. The order parameters for this *equilibrium* transition are the shear and deviatoric strains (e_3, e_2). Our earlier MD work on microstructure selection[16], addressed the issue of dynamical selection from a more mesoscopic point of view. Though we focus on a model solid-solid transformation, our conclusions should hold very generally.

A "quench" from the square parent phase across the structural transition, nucleates rhombic regions; the shapes, microstructure, and nucleation dynamics of product nuclei depend on the 'depth-of-quench' (Fig.1a). A quench into region F (ferrite), results in a critical nucleus which is isotropic, untwinned and with a rhombic microstructure separated by grain boundaries (Fig.1b). In contrast, a quench into region M (martensite), nucleates a 'needle-like' region – the critical nucleus is highly anistropic, with the long axis lying along one of the axes of the parent square lattice (Fig.1c). The microstructure is twinned — a plot of the shear strain e_3 reveals that it changes sign across a twin interface between two degenerate product variants which lies along one of the square axes. The regions F and M are separated by a *dynamical phase boundary*, as seen from the sharp jumps of (i) the shape anisotropy [16] and (ii) the degree of twinning of the critical nucleus, at the transition (Fig.1d). In both phases, the nucleation of the product is accompanied by the formation of nonaffine zones (NAZ) characterized by a large value of the nonaffine parameter ϕ, derived from elastic strains by coarse-graining the particle displacements [17] – the M and F nuclei exhibit a distinct patterning and dynamics of the NAZs [16]. We emphasize that this dynamical phase boundary is sharp only when the quench rate is infinitely fast.

We now look for signatures of this dynamical transition in the microscopic trajectories of particles. We find that the nucleation and growth of the product is initiated by the movement of a fraction of particles, which we term *active*. The clusters formed by these active particles define *dynamical heterogeneities* in the transforming solid. We find that the dynamical heterogeneities so defined, overlap completely with the more coarse grained NAZs.

A closer look at the space-time trajectories within and

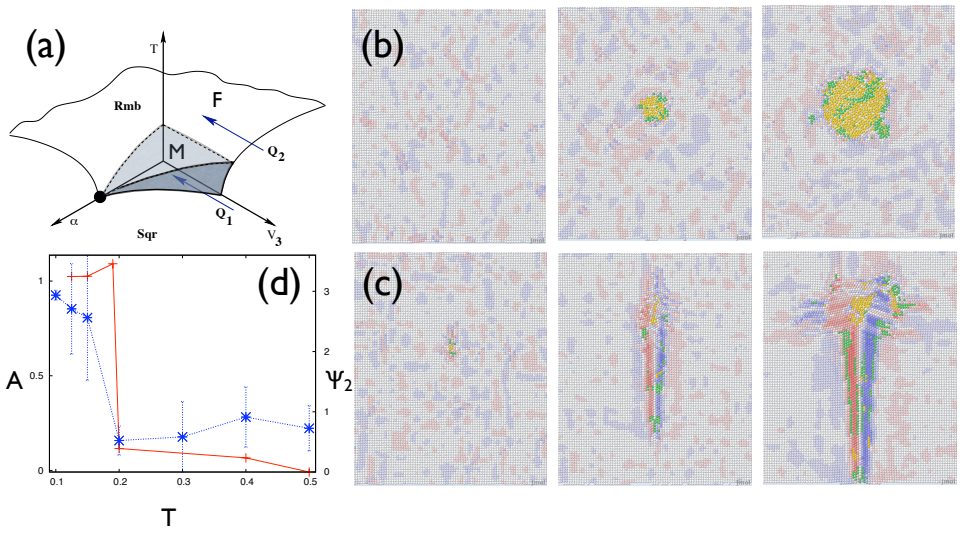

FIG. 1: (a) Phase diagram in $T - v_3 - \alpha$ at $\langle\rho\rangle = 1.05$, indicating the *equilibrium* $P4m \rightarrow P2$ (Sqr→Rmb) first order phase transition (curved surface bounded by solid lines) as well as the *dynamical transition* between ferrite (F) and martensite (M) (shaded surface). Particles interact via an effective (purely repulsive) short range potential - a sum of an anisotropic 2-body potential (anisotropy parametrized by α) and a 3- body potential, whose strength is parametrized by v_3[16, 17]. The large black dot on the α axis denotes a tricritical point where the jump in the order parameter e_3 vanishes. (b) Snapshots of the growing F nucleus at temperature $T = 0.7$ following the quench (Q_2, see (a)) to the F-phase at times $t = .1, 1$, and 5 (all units defined in[17]). (c) Snapshots of the growing twinned nucleus following the quench (Q_1, see (a)) to the M-phase at $T = 0.1$ at comparable values of t . The colors denote e_3 and the nonaffine parameter ϕ [16, 17], Red $\rightarrow e_3 > 0$, Blue $\rightarrow e_3 < 0$, Gold $\rightarrow \phi > 0$ and Green $\rightarrow \phi < 0$. (d) *Shape anisotropy* A (blue $*$, axis on the left) and the *degree of twinning* Ψ_2 (red $+$, axis on the right) of the product nucleus, (for definitions see [17]) vs. T, shows an abrupt jump across the dynamical transition.

in the vicinity of the dynamical heterogeneities in the form of *kymographs* (Fig.2a), reveals fine differences between the M and F -phases. In the M-phase, we see that nucleation is accompanied by the birth of a small fraction of active particles, surrounded by regions of inactive particles [5]. At these early times they move ballistically and in a coordinated manner; the velocity correlation is significant both along a single trajectory and across neighboring trajectories at equal time. The number of active particles grows with time, with the older active particles seeding newer ones. Note that the highly coordinated military movement, characteristic of a martensite, is apparent in these kymographs (Fig.2a and [17]). In the F-phase, the fraction of active particles is larger and their trajectories intersect many times[17]; the single particle trajectories are diffusive over time scales larger than the velocity correlation time. Indeed we find that the tagged-particle diffusion coefficient is large and athermal (Fig.2b) and is driven by local variations in free-volume as a result of accomodation [16].

The active particle trajectories show alternate arrest and movement, both in the F and M phases (Fig.2b), thus particles continuously transform from an active to inactive state. We study the statistics of such activity transitions in the two phases; the distribution of these state reversals (Fig.2c) is exponential, with a possible stretching in the F-phase. Note that the arrest of all active particles within a dynamical heterogeneity happens roughly simultaneously (Fig.2c). This is the space time realization of the observed jamming and flow[9] in the stress-flow curves within the NAZs [16].

The active particles in the M-phase are dynamically hindered and do not explore local configuration space. This is dramatically apparent in the topography of the local energy landscape set by the inactive particles, which we compute by using the fitted local order parameter, $e_3(x, y)$ in a nonlinear elastic free energy density (Fig.3) – this shows deep ridges in the local free-energy landscape, which herd active particles along a narrow channel, creating string-like excitations[10]. The width of the string is of the order of the lateral scale of the dynamical heterogeneities. In the F-phase, the landscape exhibits many criss-crossing shallow ridges which directs particles here and there, ending up in a large scale topography akin to a delta. The delta spans out isotropically, leading to diffusive collective excitations. Thus the difference in the space-time trajectories arises from the kinetic constraints on active particles created by the energy landscape due to inactive particles.

To quantify the abrupt changes in the nature of trajectories of (a few) active particles moving in the confining potential created by the (majority) inactive particles, we take a space-time approach[4, 5] and define a thermodynamics of phase transitions in trajectory space. The Lagrangian displacements $u_{i\alpha}(t) = r_{i\alpha}(t) - r_{i\alpha}(t - \delta t)$, where $\alpha = 1, 2$ (along x and y directions for the square-

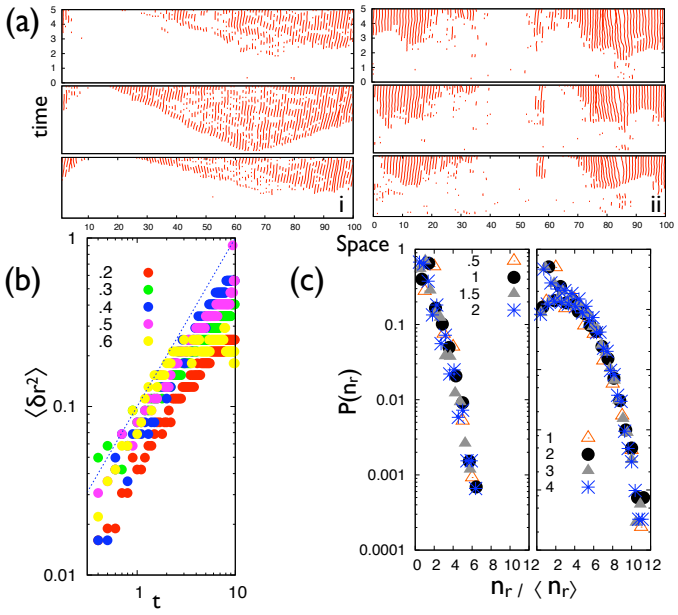

FIG. 2: (a) Space-time *kymographs* denoting particle trajectories, i.e., plots of $y(t)$ for particles at fixed values of x, showing clusters of active particles surrounded by inactive particles (empty patches). (i) Kymographs in the M-phase, $T = 0.1$, at $x = 10, 15, 20$ (top to bottom panels) and (ii) Kymographs in the F-phase, $T = 0.6$, at $x = 15, 26, 57$ (top to bottom). Active particles in M are concentrated near the edge of the single growing nucleus, while in F, they are distributed throughout the sample. The movement of active particles is ballistic in M and random in F[17]. The alternate cycles of (in)activity and the collective active (unjamming) $\rightarrow$ inactive (jamming) are apparent in the kymographs. (b) Tagged particle diffusion coefficient, obtained from the slope of $\langle \delta r^2 \rangle = \int_0^t \sum_i (\mathbf{r}_i(t') - \mathbf{r}_i(t' - \Delta t'))^2 dt'$ vs. t with $\Delta t' = 0.1$ (sum is over all active particles), is independent of temperature, over the range $T = .2 - .6$ in the F-phase. (c) Statistics of (in)active interconversions in terms of the probability distribution $P(n_r, t)$ for the number of reversals n_r (experienced by all particles from active to inactive and vise-versa) upto time t, plotted against n_r, for different times ($t = 0.5 - 2.0$ for the M-phase at $T = 0.1$ (left), and $t = 1. - 4.$ for the F-phase at $T = 0.6$ (right)). The data collapse shows that $n_r/\langle n_r \rangle$ is the scaling variable, where $\langle n_r \rangle$ is the mean number of reversals upto time t. In both phases, $P(n_r, t)$ decays exponentially, with a possible stretching in the F-phase.

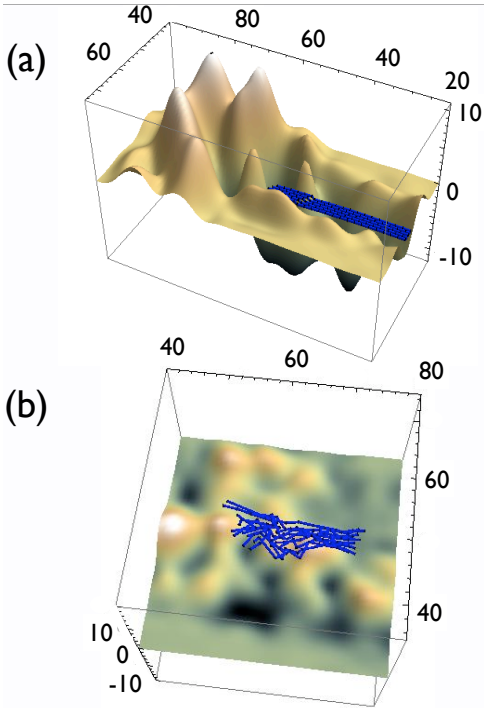

FIG. 3: Topography of local energy landscape due to the inactive particles, showing deep ridges and shallow delta in the M (a) and F (b) phases, respectively. The energy landscape is obtained by using the fitted local strain $e_3(x, y)$ in the usual (local) nonlinear elastic free energy density $ae_3^2 - be_3^4 + ce_3^6$, where coefficients a, b, c are proportional to the elastic moduli obtained explicitly from total energy calculations (see [15], for details). In (a) the deep ridge directs rows of active particles (blue lines) along a specific channel. (b) In the F-phase, the active particle trajectories span out isotropically. Thus the collective excitations are string-like in the M-phase (a) and diffusive in the F-phase (b).

to-rhombus transition) and δt is a small time offset. The active particles move 'freely' in the confining potential set by the inactive particles, thus the probability distribution of trajectories of active particles is given by $P[\mathcal{C}] \propto \exp(-S[\mathcal{C}])$[6, 7], where the 'stochastic action' is given by,

$$S[\mathcal{C}] = \int_0^{t_{obs}} \frac{1}{2D} \sum_{i,\alpha} (\tau_m \ddot{u}_{i\alpha} + \dot{u}_{i\alpha})^2 \, dt \,, \qquad (1)$$

upto an observation time, t_{obs}. Here D is a diffusion coefficient and the summation is over active particles alone subject to the constraint that the inactive particles make large portions of configuration space inaccessible [20]. This constraint can be expressed as an effective confining potential experienced by the active particles, which augments the 'free particle' action by a term of the form, $-\int_0^{t_{obs}} \sum_{i\alpha\beta} [V_{\alpha\beta} u_{i\alpha}(t) u_{i\beta}(t) + \ldots] \, dt$.

The two phases F and M are characterized by the space-time intensive off-diagonal order parameter, constructed from the bilinear $\Delta^i_{\alpha\beta}(t) = u_{i\alpha}(t) u_{i\beta}(t)$ with $\alpha \neq \beta$,

$$\mathcal{O}/N \equiv \frac{1}{t_{obs} N} \int_0^{t_{obs}} dt \sum_i |\Delta^i_{\alpha\beta}(t)|^2 \,. \qquad (2)$$

The typical value of $\mathcal{O}/N$ is zero in the M-phase and undergoes a sharp jump of $O(1)$ in the F-phase (Fig.4a-c). The order parameter probability distribution $P(\mathcal{O})$, is exponential in the M-phase with a peak at $\mathcal{O} = 0$, and changes over to a distribution with a peak at $\mathcal{O}_{max} \neq 0$ in the F-phase. To declare this a bona-fide space-time phase transition, the distribution $P(\mathcal{O})$ should exhibit

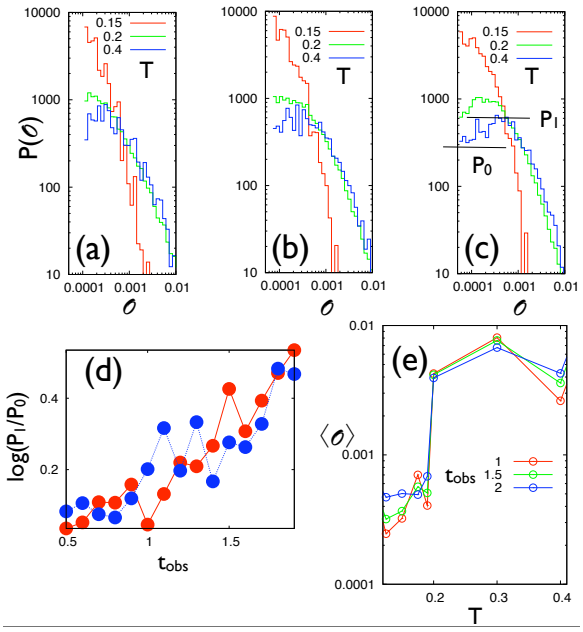

FIG. 4: (a) -(c) Probability distribution of the off-diagonal order parameter $P(\mathcal{O})$ for $T = 0.15, 0.2$ and 0.4 for $t_{obs} = 1$ (a), 1.5 (b) and 2 (c). Note the development of a peak at $\mathcal{O}_{max} \neq 0$ for $T > 0.2$, as t_{obs} increases. (d) Finite-size scaling in space-time, measured by $\log(P_1/P_0)$ versus t_{obs}, where P_1 is the probability at the maximum value $\mathcal{O}_{max}$ and $P_0 = P(0)$ shown for two temperatures $T = 0.3$ (blue circles) and 0.4 (red circles). The transition sharpens with increasing t_{obs}. (e) Mean $\langle\mathcal{O}\rangle$ as a function of T for $t_{obs} = 1, 1.5$ and 2 shows a sharp transition at $T \approx 0.2$ (compare Fig.1d).

"finite-size" scaling, with respect to changes in the space-time "volume" Nt_{obs}. This is most apparent in the scaling behaviour of $\log(P_1/P_0)$ (Fig.4d), where $P_0 = P(0)$ and $P_1 = P(\mathcal{O}_{max})$. In an equilibrium Ising phase transition, the analogous quantity measures the free-energy of domain-walls and increases as L^{d-1}, where L is the linear system size and d the dimensionality of space[18]. Figure 4d shows that $\log(P_1/P_0)$ increases as t_{obs} increases, and thus scales with the "volume" of space-time, indicating that the $M - F$ transition becomes sharper in the space-time thermodynamic limit. The mean $\langle\mathcal{O}\rangle$ shows a sharp jump (Fig.4e) at the same temperature where the structural order-parameters at the mesoscopic scale, viz., A and Ψ_2, show sharp changes (Fig.1d).

Our work provides the physical link between microscopic particle trajectories and mesoscopic microstructure of the product solid, mentioned in the introduction. Our study on the dynamics of solid nucleation also reveals hitherto unsuspected connections with the physics of glass[4, 5, 10], granular media and jamming[11–13] and plasticity[8, 9]. We hope to pursue the many ramifications that these links promise, e.g., the spatiotemporal statistics of dynamical heterogeneities leading to intermittent jamming and flow; developing a nucleation theory of solid state transformations arising from string-like excitations; and formulating an explicit Landau theory to describe the thermodynamics of phase transitions in trajectory space.

Acknowledgments

SS and MR acknowledge support from DST (India) and HFSP, respectively.

[1] R. W. Cahn and P. Haasen *Physical Metallurgy* (North-Holland, Amsterdam,1996).
[2] R. Phillips *Crystals, Defects and Microstructures: Modeling Across Scales* (Cambridge University Press, Cambridge, 2001).
[3] K. Bhattacharya *Microstructure of Martensite: Why It Forms and How It Gives Rise to the Shape-Memory Effect* (Oxford University Press, Oxford, 2003)
[4] L. O. Hedges, R. L. Jack, J. P. Garrahan and D. Chandler, Science **323**, 1309-1313 (2009).
[5] M. Merolle, J. P. Garrahan and D. Chandler, Proc. Natl. Acad. Sci. U.S.A. **102**, 10837-10840 (2005).
[6] S. Edwards, J. Stat. Phys. **116**, 29-42 (2004).
[7] E. G. D. Cohen, J. Stat. Mech. P07014 (2008) .
[8] M. L. Falk and J. S. Langer, Phys. Rev. E **57**, 7192-7205 (1998) .
[9] C. E. Maloney and A. Lemaître, Phys. Rev. E, **74**, 016118 (2006).
[10] J. S. Langer, Phys. Rev. Lett. **97**, 115704 (2006).
[11] A. J. Liu and S. R. Nagel, Nature **396**, 21-22 (1998).
[12] F. Lechenault, O. Dauchot, G. Biroli and J. P. Bouchaud, Europhys. Lett. **83**, 46003 (2008).
[13] R. Candelier and O. Dauchot, arXiv:0906.2679 (2009).
[14] M. Rao and S. Sengupta, Phys. Rev. Lett. **91**, 045502 (2003).
[15] M. Rao and S.Sengupta, J.Phys.: Cond. Mat **16**, 7733-7752 (2004).
[16] J. Bhattacharya, A. Paul, S. Sengupta and M. Rao, J. Phys.: Condens. Matter **20**, 365210 (2008).
[17] EPAPS supplementary text.
[18] K. Binder, Z. Phys. B - Condensed Matter **43**, 119-140 (1981).
[19] D. Frenkel and B. Smit, *Understanding Molecular Simulations* (Academic Press, San Diego, 1996).
[20] There is a further constraint : in the absence of external forces, the centre of mass displacement of the system should be zero.